Visualization and Analysis Tools for Low-Frequency Propagation in a Generalized 3D Acoustic Space*

ADAM J. HILL, *AES Student Member*, **AND MALCOLM O. J. HAWKSFORD**, *AES Fellow*
(ajhilla@essex.ac.uk) (mjh@essex.ac.uk)

University of Essex, School of Computer Science & Electronic Engineering, Colchester, Essex, CO4 3SQ, UK

A software toolbox is described that enables three-dimensional animated visualization and analysis of low-frequency wave propagation within a generalized acoustic environment. The core computation exploits a finite-difference time-domain (FDTD) algorithm selected because of its known low-frequency accuracy. Multiple sources can be configured and analyses performed at user-selected measurement locations. Arbitrary excitation sequences enable virtual measurements embracing both time-domain and spatio-frequency-domain analyses. Examples are presented for a variety of low-frequency loudspeaker placements and room geometries to illustrate the utility of the toolbox for various acoustical design challenges.

0 INTRODUCTION

There are numerous aspects of room acoustics that must be taken into consideration when configuring a loudspeaker system for the ideal acoustical performance. A software package, or toolbox, that provides in-depth visualization and analysis of room acoustics while also providing means of virtually prototyping low-frequency room correction techniques can be beneficial in the design process. In particular the low-frequency behavior in small enclosed spaces can vary wildly within a small listening area, presenting the need for a practical analysis tool.

The toolbox utilizes the strengths of the finite-difference time-domain (FDTD) simulation method, which is well known in electromagnetics [1] and has been gaining steady popularity in acoustics, facilitated by increases in available computational power, resulting in highly accurate low-frequency simulations [2]–[5]. The toolbox presented in this engineering report assimilates previous work concerning acoustical simulation and analysis into an intuitive package, allowing for maximum control over the virtual acoustical and electrical environments.

In addition to describing the computational core of FDTD, the multitude of functions integrated within the toolbox will be highlighted. The techniques for enabling nonrectangular room and obstacle simulation will also be described in detail to demonstrate how FDTD's architecture is well matched to nonrectangular simulations. The flexible nature of the toolbox enables accurate acoustic modeling that extends from small-room acoustics to large-scale sound reinforcement where low-frequency problems, albeit very different in nature, can exist without a properly configured system. Multiple examples will be presented, showcasing the capabilities of the toolbox as well as the overall advantages of using a toolbox of this nature in acoustical and audio engineering work.

The software presented here, although capable of supporting a wide range of applications, was originally created to serve as a powerful tool for the authors' ongoing research into low-frequency control [6], [7]. Consequently, in order to stimulate further development and to allow interested parties to apply the existing toolbox to their own work, a condensed version is available for free download [8]. The intention is to let this software evolve as an open-source project to assist acoustics research. Individuals are therefore invited to submit routine improvements and additions and also to report on their applications and projects.

1 FDTD SIMULATION METHOD

A core appeal of FDTD acoustic simulation is that it operates directly in the time domain, allowing for transient analysis and simple conversion to the frequency domain [3]. FDTD operates with a discretized sound wave equation in the temporal and spatial frequency domains. The resulting set of partial differential equations governs the simulation, which operates over a spatially and temporally staggered set of grids containing sound pressure and particle velocity data as depicted in Fig. 1. Staggered grids are required due to the update procedure, which requires an interlacing of adjacent particle velocity values for pressure updates and adjacent pressure values for particle velocity updates.

*Presented at the 127th Convention of the Audio Engineering Society, New York, 2009 October 9–12; revised 2011 January 12 and April 15.

This grid layout allows for a simple placement of sources within the simulated space where any grid point can be defined as a source location. Similarly, any grid point can be designated as a listening location, allowing for received signals to be recorded and analyzed. The nonboundary particle velocity update procedure described by Eq. (1) can be applied over the entire grid in one step, a technique that greatly facilitates computational efficiency,

$$u^x_{x+\frac{\Delta x}{2},y,z}\left(t+\frac{\Delta t}{2}\right)=u^x_{x+\frac{\Delta x}{2},y,z}\left(t-\frac{\Delta t}{2}\right)-\frac{\Delta t}{\rho\Delta x}\left[p_{x+\Delta x,y,z}(t)-p_{x,y,z}(t)\right] \quad (1)$$

where u denotes the particle velocity components at a grid point specified by x, y, z and time t. Grid points are spaced according to Δx and are updated at intervals corresponding to the time step Δt. The speed of sound and the air density are represented by c and ρ, respectively.

The corresponding nonboundary equations for both y- and z-dimension particle velocity updates can be formed by altering the x-dimension equation (where the FDTD equations have been adapted from [2], [3], [5]).

The pressure grid can then be updated from the particle velocity grids using the equation

$$\begin{aligned}p_{x,y,z}(t+\Delta t)=p_{x,y,z}(t)&-\frac{c^2\rho\Delta t}{\Delta x}\left[u^x_{x+\frac{\Delta x}{2},y,z}\left(t+\frac{\Delta t}{2}\right)-u^x_{x-\frac{\Delta x}{2},y,z}\left(t+\frac{\Delta t}{2}\right)\right]\\&-\frac{c^2\rho\Delta t}{\Delta y}\left[u^y_{x,y+\frac{\Delta y}{2},z}\left(t+\frac{\Delta t}{2}\right)-u^y_{x,y-\frac{\Delta y}{2},z}\left(t+\frac{\Delta t}{2}\right)\right]\\&-\frac{c^2\rho\Delta t}{\Delta z}\left[u^z_{x,y,z+\frac{\Delta z}{2}}\left(t+\frac{\Delta t}{2}\right)-u^z_{x,y,z-\frac{\Delta z}{2}}\left(t+\frac{\Delta t}{2}\right)\right] \quad (2)\end{aligned}$$

where p represents the sound pressure components.

Particle velocity grid points adjacent to boundaries are not fully surrounded by pressure points, as required in Eq. (2). A special set of boundary condition equations must be utilized to update these particle velocity grid points. The update equation for the x-dimension particle velocity component is given by Eq. (3), which can be adjusted for use with the remaining dimensions,

$$u^x_{x,y,z}\left(t+\frac{\Delta t}{2}\right)=\frac{R_x-Z}{R_x+Z}u^x_{x,y,z}\left(t-\frac{\Delta t}{2}\right)+\frac{2}{R_x+Z}p_{x,y,z}(t) \quad (3)$$

with

$$Z=c\rho\frac{1+\sqrt{1-\alpha}}{1-\sqrt{1-\alpha}} \quad (4)$$

$$R_x=\frac{\rho\Delta x}{\Delta t} \quad (5)$$

where Z is the characteristic wall impedance and α the boundary absorption coefficient. These boundary conditions produce frequency-independent surfaces where the absorption of each surface can be controlled independently. Since surface absorptive properties can vary considerably over the audible frequency range, these equations can be expanded to consider frequency-dependant and reactive surfaces, as demonstrated in [5]. However, because current research [6], [7] is focused only on subwoofer applications (below ~120 Hz), frequency-independent absorption is sufficient due to the relatively narrow frequency band of interest. Should frequency-dependent absorption be required, this can be facilitated using recursive filters to endow each boundary element with memory.

In order to avoid spectral and/or spatial aliasing, care must be taken when defining the grid spacing and simulation time step. A smaller time step will allow for accurate simulations up to a higher frequency, as governed by the Nyquist frequency, which requires there to be at least two sample points per frequency period in the time domain to reproduce the signal accurately. Less than two sample points per period will introduce aliasing where the frequency is folded back over the Nyquist frequency, causing incorrect identification of a component at a lower frequency [9].

In addition the grid element spacing must be sufficiently less than the smallest wavelength within the bandwidth of interest. It has been suggested that reasonable results can be achieved by allocating at least five to ten grid elements per wavelength [3]. A spacing of 0.1 m, for example, gives accurate results below 600 Hz by the measure of five elements per wavelength. Although spatial sampling theory ultimately binds the maximum grid spacing, overly wide spacing introduces additional error into the iterative computation, thus a more conservative grid layout is required in practice.

The necessary time step must be calculated to ensure stability based on the grid element spacing, which is defined by the user in this particular application. It is important, therefore, to choose a time step that corresponds to the element spacing, both to allow for accurate

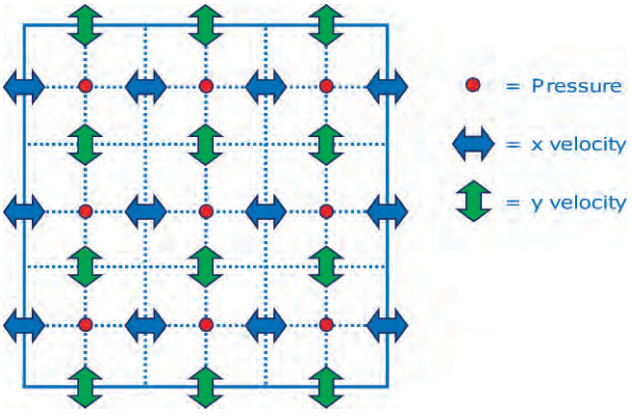

Fig. 1. Staggered-grid layout for two-dimensional FDTD simulation.

sound wave propagation and to minimize grid dispersion errors. This can be calculated using the equation [3], [5]

$$c\Delta t \leq 1/\sqrt{\frac{1}{\Delta x^2}+\frac{1}{\Delta y^2}+\frac{1}{\Delta z^2}}. \quad (6)$$

Since Eq. (6) estimates the maximum time step allowed for system stability, it can be used to ensure both stability and maximum computational efficiency.

2 FDTD SIMULATION OF NONRECTANGULAR SPACES

Since FDTD operates using a collection of grids with points around edges defined as boundaries, simulations can be readily modified for nonrectangular topologies. This is accomplished by deriving a set of masks for the pressure and particle velocity grids. The masks are a set of grids that correspond to the pressure and particle velocity grids used in the simulation. When the corresponding mask value for a simulation grid point has a value of 1, that point will be included in the simulation space, whereas a mask value of 0 will exclude that particular grid point from the simulation space, as illustrated in Fig. 2.

In this study the pressure grid mask is defined initially by the user [Fig. 3(a)]. Since particle velocity updates at boundaries require neighboring pressure points for proper calculation, masks must be generated that embrace the required pressure points for boundary conditions [Fig. 3(c)].

Separate *x*- and *y*-particle velocity element grid masks must be generated from the user-defined pressure element grid mask since the grids all have different dimensions, as illustrated in Fig. 1. A pressure element grid of dimensions 20×20 (*x* by *y*) corresponds to an *x*-particle velocity element grid of dimensions 21×20 and a *y*-particle velocity element grid of dimensions 20×21. This is because pressure elements are always surrounded by particle velocity elements, requiring an additional element in each primary dimension.

With this in mind, particle velocity masks are generated from the pressure mask by first searching the pressure mask for any nonzero values. The corresponding indices of these nonzero values are then addressed in the particle velocity mask matrices (initialized to all 1s) so that these indices are set to zero (outside the nonboundary element set) along with an additional

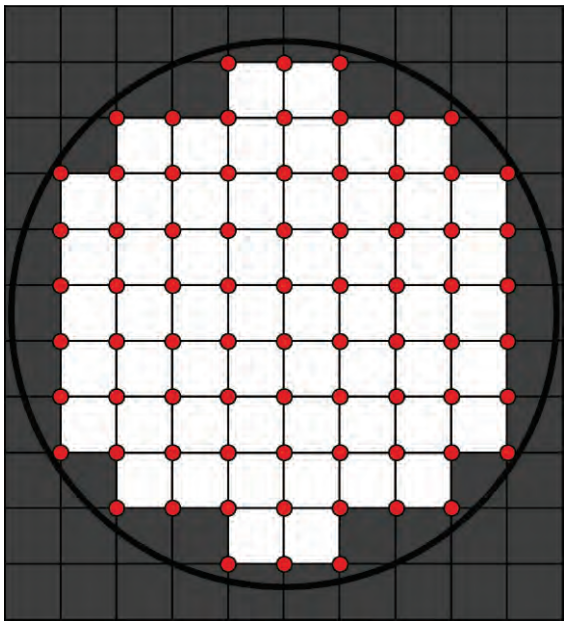

Fig. 2. Simple discretization of element grid for circular two-dimensional space. ●—pressure elements.

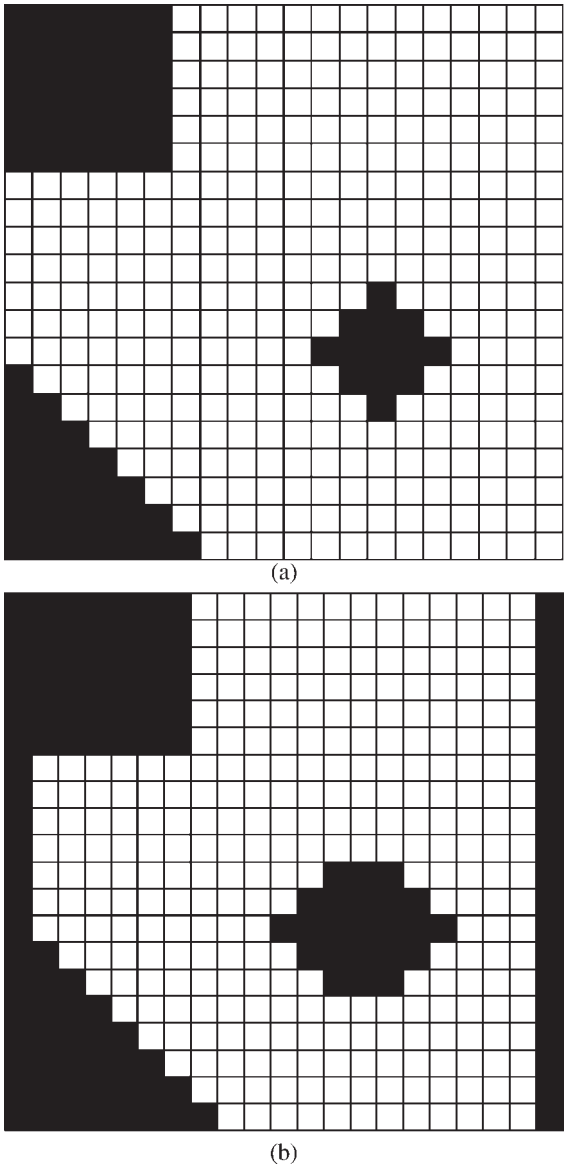

Fig. 3. (a) 20×20 user-defined pressure mask. (b) 21×20 *x*-dimension nonboundary particle velocity mask. (c) 21×20 *x*-dimension boundary condition particle velocity mask. White—inside room; black—outside room.

zeroed element adjacent to the final pressure mask defined as a zeroed element in the positive moving direction [Fig. 3(b)].

Next the generated nonboundary particle velocity masks can be used to generate boundary masks which indicate the particle velocity elements that must be updated with the boundary element equations. These masks are generated by inspecting the nonboundary masks and setting any elements marked outside the space, but adjacent to an element within the space, to be inside the boundary space (set to 1). All other elements are set to zero (outside the boundary space). These masks are valid for use within all particle velocity boundary condition update equations [Fig. 3(c)].

An advanced method for nonrectangular topology simulation employs a locally conformal grid layout to help reduce sound wave scattering errors. This technique, proposed in [5], allows for variable element spacing, which can be used to provide a denser concentration of elements near room boundaries where scattering accuracy is crucial, while keeping element density as low as possible for nonboundary conditions to ensure computational efficiency (Fig. 4). This technique reduces high-frequency simulation errors, but has not been applied to this work since this particular software is focused exclusively on low-frequency simulations.

3 FDTD SIMULATION TOOLBOX

The described FDTD simulation technique in the preceding has been implemented within a self-contained software routine (a toolbox as defined within the MathWorks MATLAB [10] software package). The user interface is designed to be intuitive, allowing parameters for room setup, source definition, simulation, analysis, auralization, and room correction method prototyping to be accessed without opening any extra windows or programs (Fig. 5).

The FDTD simulation toolbox allows for simulation of a generalized two- or three-dimensional space containing any number of obstacles (user-defined shapes and frequency-independent absorptive properties). During the simulation, animations of the pressure distribution over time can be displayed by plotting the sound pressure grid [p in Eq. (2)]. Upon completion of the simulation a number of analysis options are available as well as an auralization function.

A user first defines the simulation space's rectangular dimensions, grid size, and absorption values (one for each individual room boundary and obstacle surface), all within the "Room Setup" area of the toolbox. Once completed, a visualization of the pressure grid is displayed in the "Room Configuration" area, allowing the user to configure the room topology as necessary using a "cookie-cutter"-like approach (Fig. 6). Other simulation parameters, including listening locations, source signal and location(s), and animation/plotting type, can be adjusted in the "Measurement Settings," "Source Settings," and "Simulation Settings" areas, respectively. Available source signals include Gaussian pulse, sinusoid, maximum-length sequence (MLS), tone bursts, swept sinusoid, and any real-world audio selection (imported from .wav files).

Various analysis options are available once the time-domain simulation is complete, including theoretical mode distribution (spatial and spectral) plotting as well

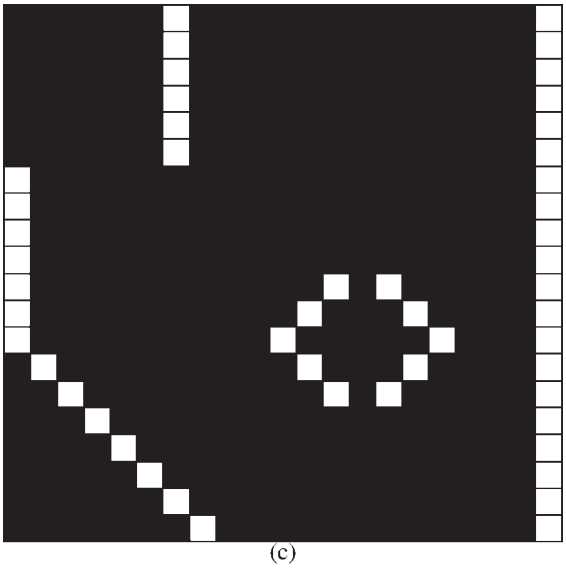

(c)

Fig. 3. *continued*

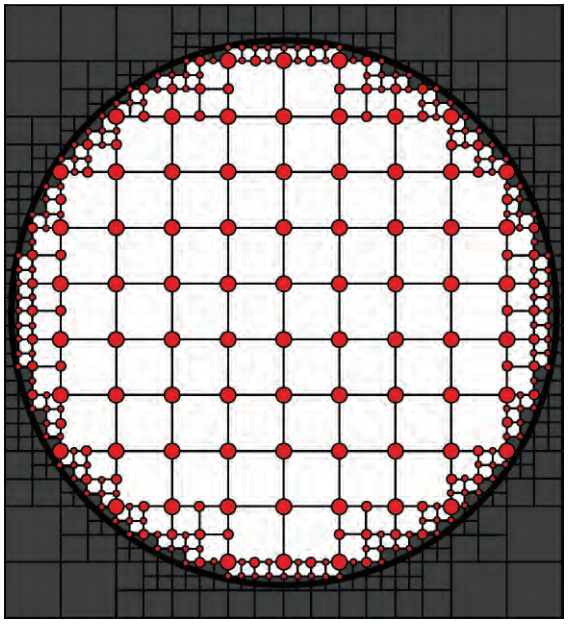

Fig. 4. Locally conformal discretization of element grid for circular two-dimensional space. ●—pressure elements.

as data plotting in time and frequency domains, spectrograms, input/output comparisons, and waveform accuracy plots (if tone burst signals are used). When performing frequency-domain analysis, two room response metrics are automatically calculated and displayed—magnitude deviation and spatial variance. Magnitude deviation MD calculates the frequency response deviation from flat (0 dB) at each measurement location

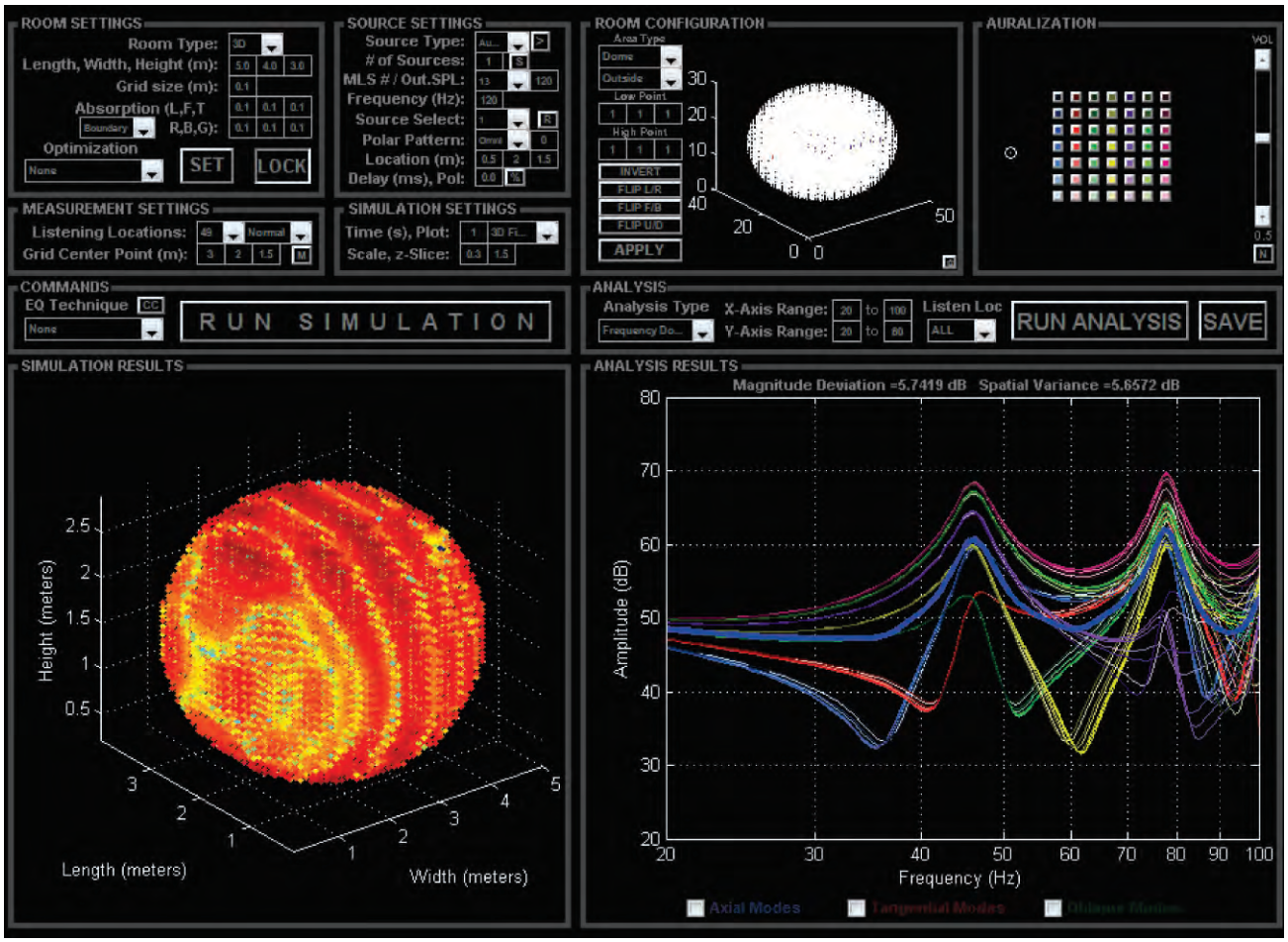

Fig. 5. FDTD simulation toolbox GUI in MATLAB.

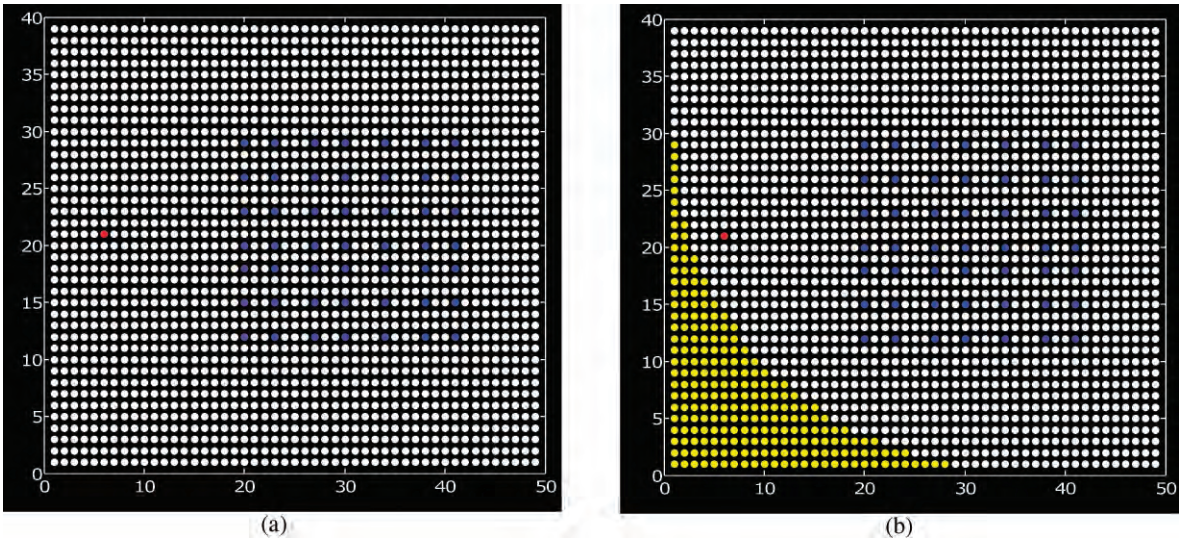

Fig. 6. Room topology modification procedure. Blue—listening locations; red—source locations; yellow—highlighted pressure points for modification.

and averages all calculated values to give a single metric [11],

$$\mathrm{MD} = \sqrt{\frac{1}{n_f - 1}\sum_{i=f_{\min}}^{f_{\max}} (x_i - \ddot{x})^2}. \quad (7)$$

Average spatial variance measures the frequency response variation from point to point within the listening space, calculated at each frequency bin for all measurement points and then averaged to give the overall spatial variance SV of the listening area [11],

$$\mathrm{SV} = \frac{1}{n_f}\sum_{i=f_{\min}}^{f_{\max}} \sqrt{\frac{1}{n_p - 1}\sum_{p=1}^{n_p}(x_{p,i} - \ddot{x})^2}. \quad (8)$$

The magnitude deviation MD is calculated over the frequency range $f_{\min}$ to $f_{\max}$, consisting of n_f frequency bins. The measured sound-pressure level at frequency bin i is represented by x_i and the mean sound-pressure level over the entire frequency range at that location is represented by $\ddot{x}$. The average spatial variance SV is calculated over all n_p listening locations where, $x_{p,i}$ represents the measured sound-pressure level at location p and frequency bin i.

Finally all simulated measurements can be auralized in the "Auralization" area of the toolbox. With the exception of source signals from .wav files, all measured signals can be auralized without any additional processing required. For the case of .wav files the signal is first frequency divided using a linear-phase complementary finite-impulse response (FIR) crossover network. The low band of the output is down-sampled to the simulation sample rate and then run through the FDTD simulation while the high band is appropriately delayed to each listening location. When the simulation is complete, the two bands are recombined into the final signal (after appropriate low-band upsampling to the original sample rate).

The following section highlights the described functionality of the toolbox and illustrates its usefulness for solving a variety of common acoustically related problems.

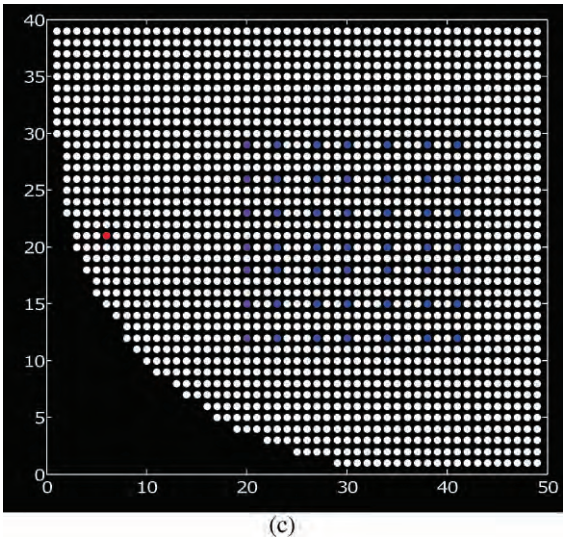

Fig. 6. *continued*

4 SIMULATION EXAMPLES

The FDTD simulation toolbox provides a comprehensive set of tools for a wide range of situations. Through the use of masking, the toolbox can readily be configured to model a variety of nonrectangular spaces (Fig. 7) or to simulate the acoustical behavior of a coupled network of rooms (Fig. 8). In addition to room topology configurability, the toolbox provides flexibility in terms of source/listening area layout and source signal manipulation.

Unless otherwise noted, all examples shown in the following sections relate to a 5 by 4 by 3 m closed space with 0.1 m grid spacing and 10% frequency-independent absorption on all surfaces.

4.1 Simulation Validation

Before analyzing data from advanced simulations, the basic functionality of the FDTD simulation method must be verified. Validation can be performed using the toolbox's visualization and analysis capabilities alongside the theoretical room-mode calculator function. This calculator operates using a simple equation based on the room's dimensions and the speed of sound [12],

$$f = \frac{c}{2}\sqrt{\left(\frac{\eta_x}{L_x}\right)^2 + \left(\frac{\eta_y}{L_y}\right)^2 + \left(\frac{\eta_z}{L_z}\right)^2} \quad (9)$$

where f is the calculated room mode (in Hz) based on the room dimensions L_x, L_y, and L_z and mode numbers η_x, η_y, and η_z. Modes with only one nonzero mode number correspond to axial modes (two surfaces involved). Two nonzero mode numbers corresponds to tangential modes (four surfaces involved), and three nonzero mode numbers gives oblique modes (six surfaces involved). This type of modal calculation is only valid for three-dimensional rectangular rooms and assumes the room to be constructed of three sets of parallel surfaces.

An impulse response was measured at each listening location within a square grid of 25, centered at (3.0 m, 2.2 m, 1.8 m) and a single omnidirectional subwoofer located at a room corner. The individual impulse responses were used to calculate the frequency response for each location and plotted with the theoretical modes displayed as vertical lines (Fig. 9).

With theoretical and simulated values in close agreement, further simulation validation was performed by comparing simulated pressure distributions at room modes to the theoretical distributions (Figs. 10–12). Again, the pressure distributions for axial, tangential,

and oblique modes agree with theory, allowing for complex simulations to be carried out with greater confidence.

4.2 Single Subwoofer Positioning

The low-frequency response of a room is altered significantly by subwoofer placement. The majority of subwoofers available commercially have omnidirectional polar patterns where the subwoofer operates as a pressure source. An omnidirectional subwoofer will cause a room to behave very differently depending on whether it is placed near a pressure node (pressure = minimum, particle velocity = maximum) or a pressure antinode (pressure = maximum, particle velocity = minimum) [13]. When placed at a node, the subwoofer exhibits very weak coupling with the room, causing the room mode to be minimally excited [Fig. 13(a)]. The opposite is true when placement is near an antinode [Fig. 13(b)] [12].

The suppressed mode shown in Fig. 13(a) corresponds to the (0, 1, 0) axial mode at 42.875 Hz. Using the room-mode calculation function to assess the two source locations tested (Fig. 14), it is clear that the corner location (0.4 m, 0.4 m, 0.4 m) is very close to an antinodal plane for 42.875 Hz, whereas the central wall location (0.4 m, 2.0 m, 0.4 m) is directly on a nodal plane. As expected, the corner location strongly excites the room mode while the central wall location causes minimal excitation.

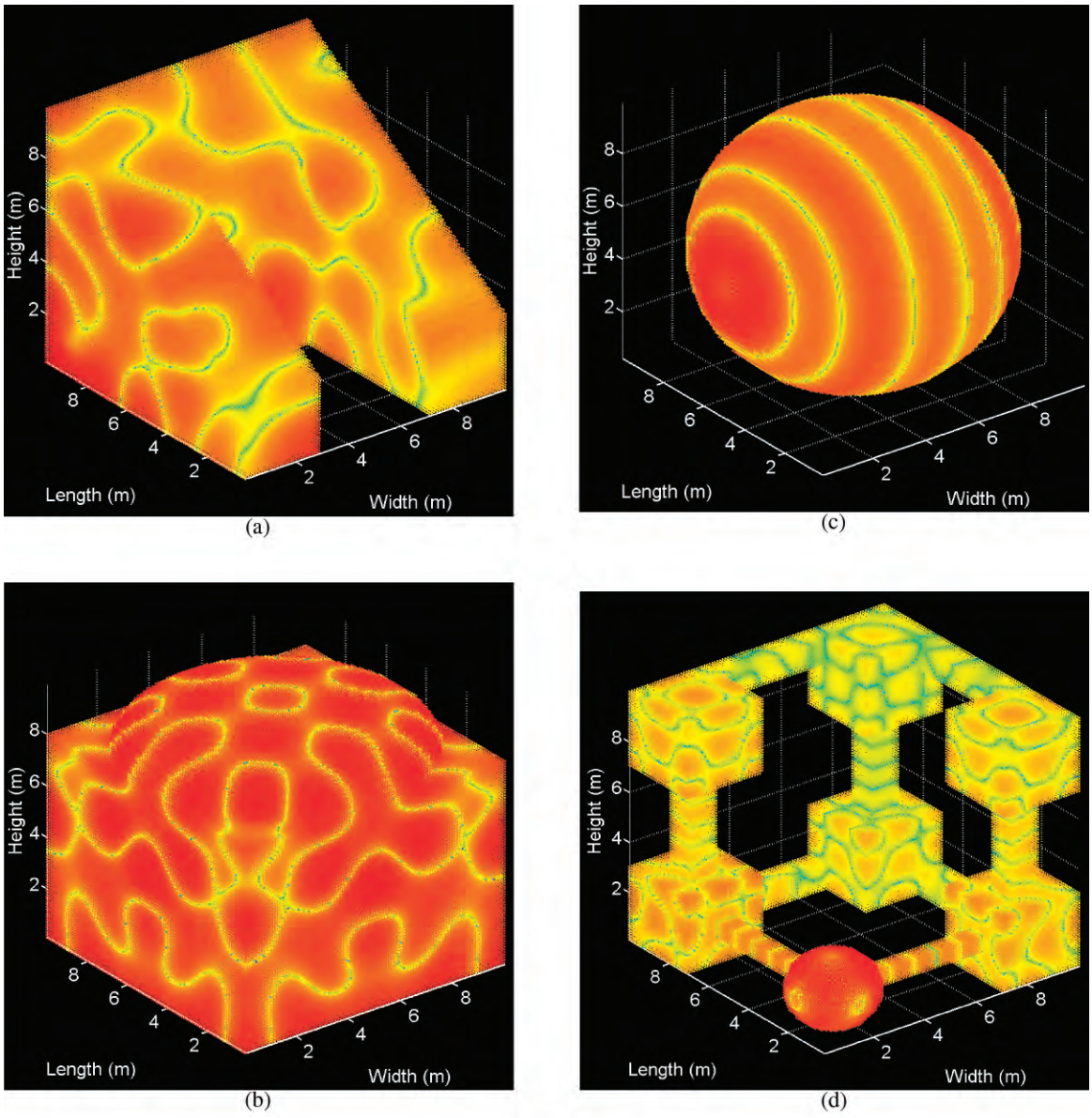

Fig. 7. Examples of nonrectangular room simulations using single source. (a) At 100 Hz, located at (1.0 m, 9.0 m, 1.0 m). (b) At 120 Hz, located at (5.0 m, 5.0 m, 1.0 m). (c) At 100 Hz, located at (1.0 m, 5.0 m, 5.0 m). (d) At 200 Hz, located at (1.5 m, 1.5 m, 1.5 m).

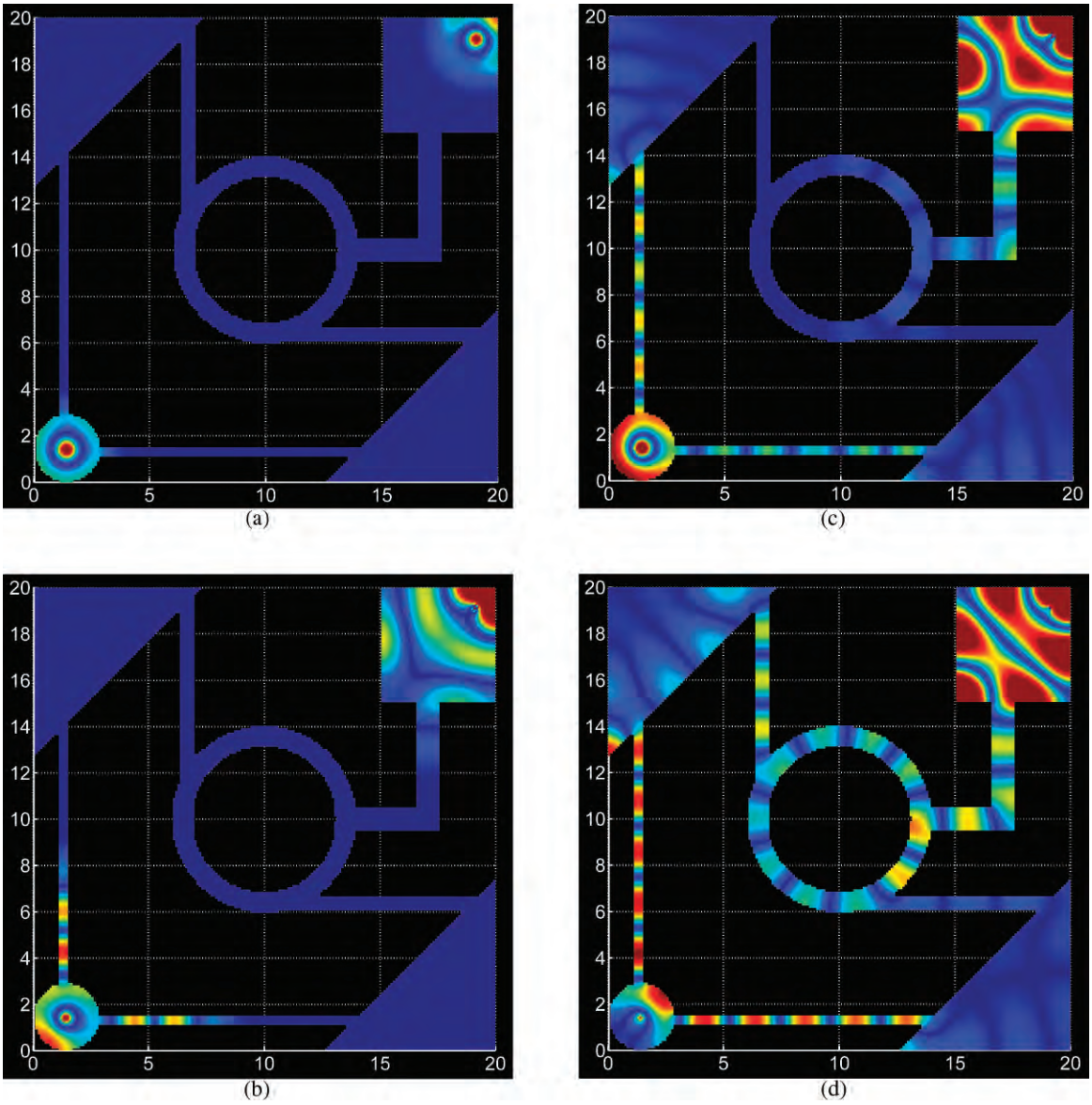

Fig. 8. Animation snapshots of simulation of a network of rooms using two sources at (1.5 m, 1.5 m) and (19.0 m, 19.0 m) driven by a constant 80-Hz sinusoidal signal. (a) 10.0 ms. (b) 25.5 ms. (c) 64.0 ms. (d) 2000 ms.

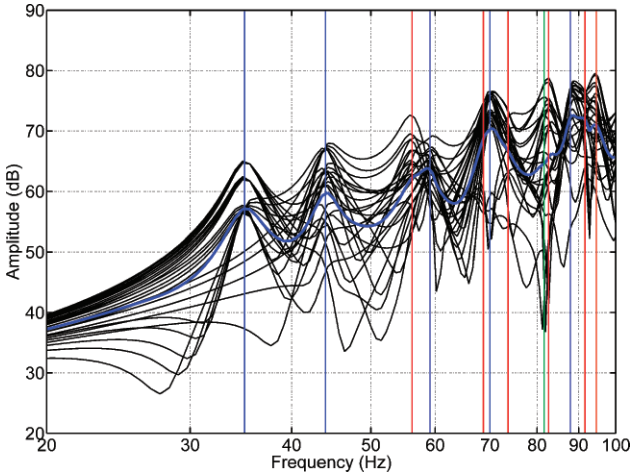

Fig. 9. Uncorrected room response due to a single omnidirectional subwoofer in room corner for 25 listening locations. Heavy blue line—average response; vertical lines—theoretical axial (blue), tangential (red), and oblique (green) modal frequencies.

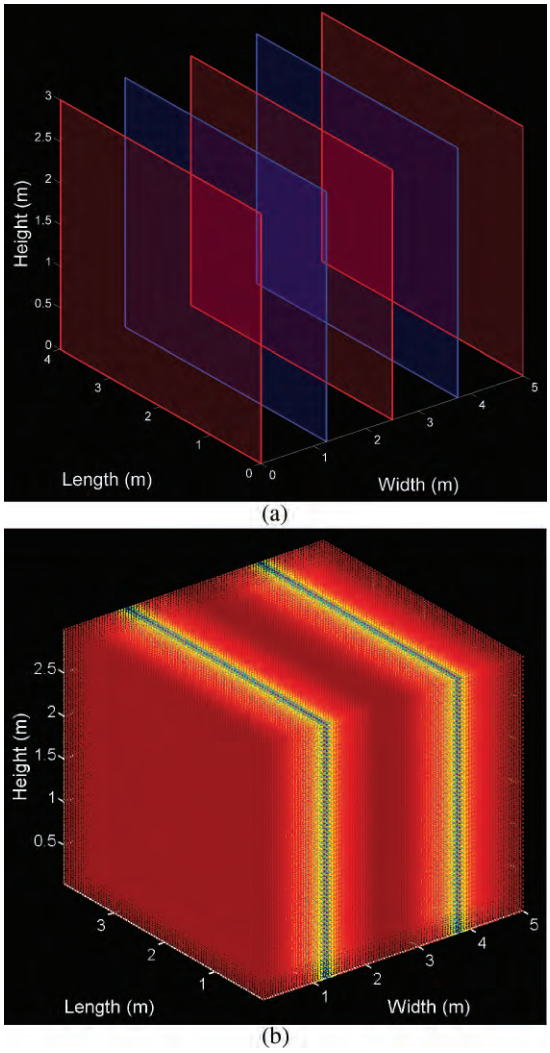

Fig. 10. Spatial pressure distribution for axial mode (2, 0, 0) at 68.6 Hz. (a) Theoretical. (b) Simulated.

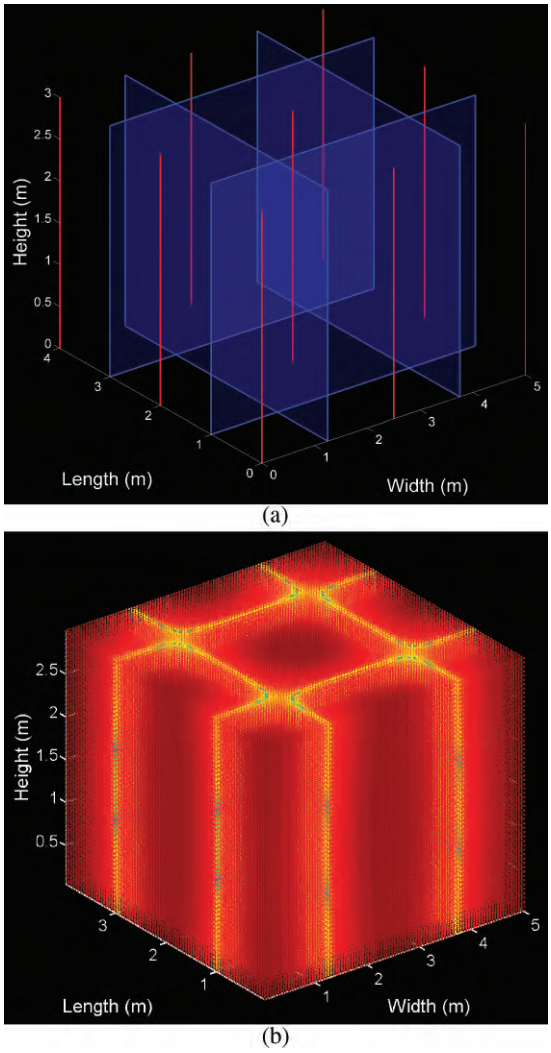

Fig. 11. Spatial pressure distribution for tangential mode (2, 2, 0) at 109.8 Hz. (a) Theoretical. (b) Simulated.

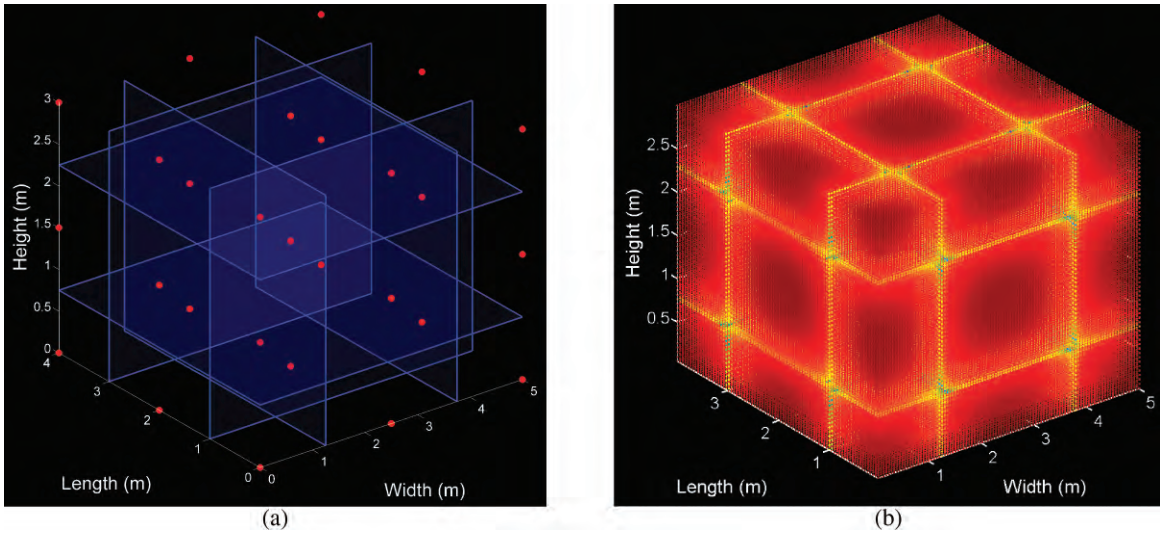

Fig. 12. Spatial pressure distribution for oblique mode (2, 2, 2) at 158.5 Hz. (a) Theoretical. (b) Simulated.

Given these results, placing the source directly in the center of the room should suppress many low-order axial modes that have antinodal points or planes at the room center (Fig. 15). The low-order modes of (1, 0, 0), (0, 1, 0), (0, 0, 1), and (1, 1, 0) have all been minimally excited due to the source's central placement.

While central placement shows increased modal suppression, the center of the room is not a practical location for a subwoofer. Consequently a source optimization routine has been provided within the toolbox to assist in locating a more practical single subwoofer location with spatial variation minimization in mind. For example, this routine is carried out allowing for placement along the *y*-axis wall with a distance range from the wall of 0.2–2.6 m (Fig. 16).

It must be noted that nodal-source placement minimizes excitation of unwanted room modes. Thus the subwoofer output is not strongly reinforced by the room due to the low room-to-source coupling. As a result the system will be less efficient, requiring higher subwoofer output capabilities, a fact that must be considered during the system design and configuration process.

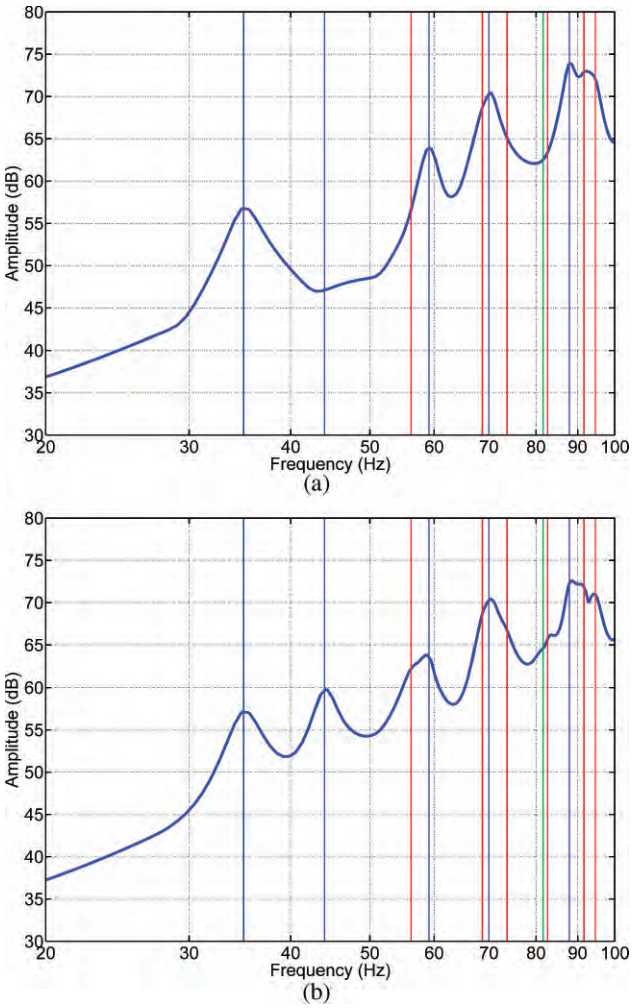

Fig. 13. Average frequency response over 25 listening locations with single omnidirectional source. (a) At (0.4 m, 2.0 m, 0.4 m). (b) At (0.4 m, 0.4 m, 0.4 m).

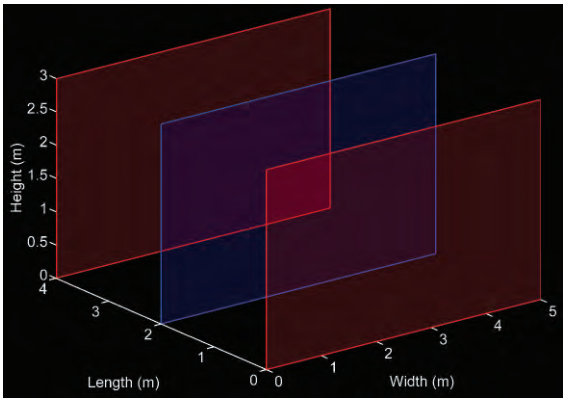

Fig. 14. Theoretical modal spatial distribution for (0, 1, 0) mode in a 5 by 4 by 3 m rectangular room. Red—antinodal plane; blue—nodal plane.

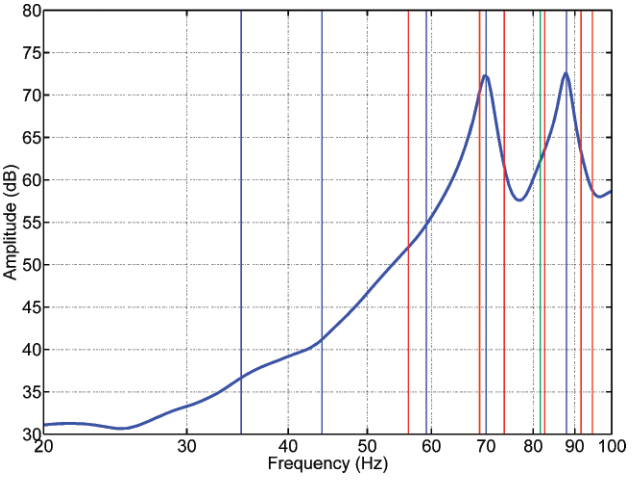

Fig. 15. Average frequency response over 25 listening locations with single omnidirectional source at (2.5 m, 2.0 m, 1.5 m).

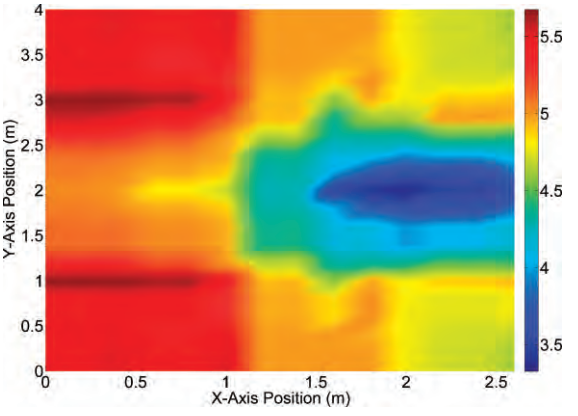

Fig. 16. Spatial variance (dB) at various single subwoofer positions within a 5 by 4 by 3 m rectangular room. Subwoofer height = 0.4 m.

4.3 Multiple Subwoofer Positioning

More often than not, subwoofer placement is restricted by practicality (such as objects present in the room), where placement of a single subwoofer at the center of a rectangular room to reduce resonances is normally an unrealistic option. The solution to this compromise scenario is to employ multiple subwoofers located at antinodal positions of opposite polarity, that is, one subwoofer is placed at a location corresponding to a positive-pressure amplitude maximum while another is placed at a negative-pressure amplitude maximum. The opposite polarity of antinodal positions will cause destructive interference, minimizing excitation [12]. This placement gives similar results [Fig. 17(a)] to placing a single subwoofer at that mode's node [Fig. 13(a)], which utilizes a single subwoofer placed at a node to achieve modal suppression due to inefficient coupling.

Two more subwoofers can be placed at the other corners to help suppress the first-order mode along the width of the room [Fig. 17(b)] and thus achieve further reduction in spatial variance.

In addition, global equalization (all drive signals processed with the same filters) applied to a single subwoofer system is problematic as although the response can be improved at certain locations, it inevitably degrades elsewhere due to low correlation between listening location responses (Fig. 18). This can only be changed by adjusting the positions of the sources or listeners or to apply individual correction to each source (for multiple subwoofer systems) [14]. However, an optimally aligned multiple-subwoofer system naturally exhibiting low spatial variance will benefit from global equalization due to higher correlation between the listening location frequency responses (Fig. 19).

4.4 Polar-Pattern Control

Another helpful feature of the FDTD simulation toolbox is the ability to experiment with polar-pattern

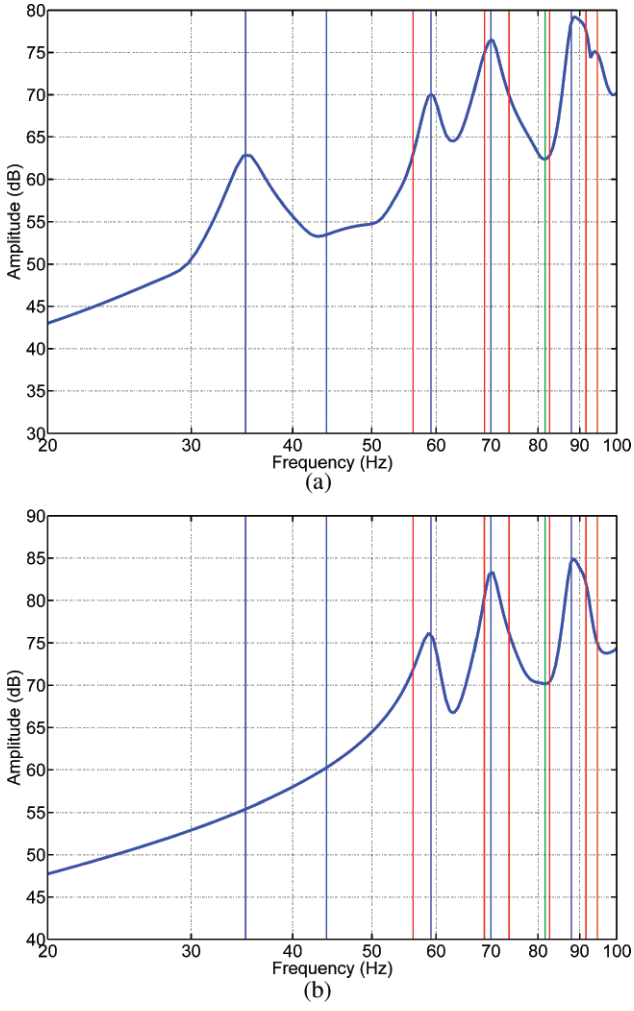

Fig. 17. Average frequency response over 25 listening locations. (a) Two omnidirectional sources at (0.4 m, 0.4 m, 0.4 m) and (0.4 m, 3.6 m, 0.4 m). (b) Four omnidirectional sources at (0.4 m, 0.4 m, 0.4 m), (0.4 m, 3.6 m, 0.4 m), (4.6 m, 0.4 m, 0.4 m), and (4.6 m, 3.6 m, 0.4 m).

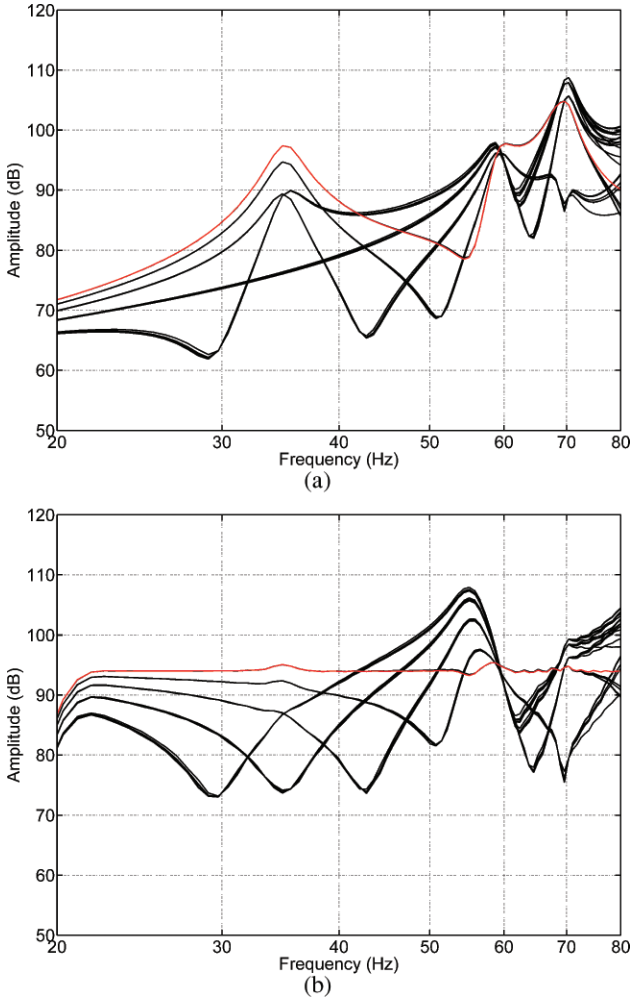

Fig. 18. Simulated frequency response over 25 listening points with single omnidirectional subwoofer at (0.4 m, 2.0 m, 0.4 m). (a) No equalization. (b) Single-point equalization at red line.

control of a source. Currently this is achieved by automatically positioning and delaying a number of point sources by means of Olson's gradient loudspeaker theory [15]. In one example two point sources are placed in an anechoic environment 0.2 m apart, with one source having reversed polarity. Individually these sources radiate omnidirectionally [Fig. 20(a)], but when driven together with a sinusoidal signal, a clear dipole pattern emerges [Fig. 20(b)]. Introducing electrical delay to the secondary source (which corresponds to the source spacing) results in a cardioid radiation pattern [Fig. 20(c)].

An additional analysis option examines the diffraction caused by loudspeaker enclosures. This analysis feature is accomplished by inserting obstacles within a room that intersect to create a box. A source is then positioned at a small opening on one side to approximate a drive unit.

Cabinet diffraction is relevant over all frequencies since the geometry of the cabinet remains unchanged; however, its manifestation differs with frequency [16]. At frequencies with wavelengths shorter than the average surface radius of the cabinet, diffraction causes lobing, thus making critical the listening angle [17], [18]. A

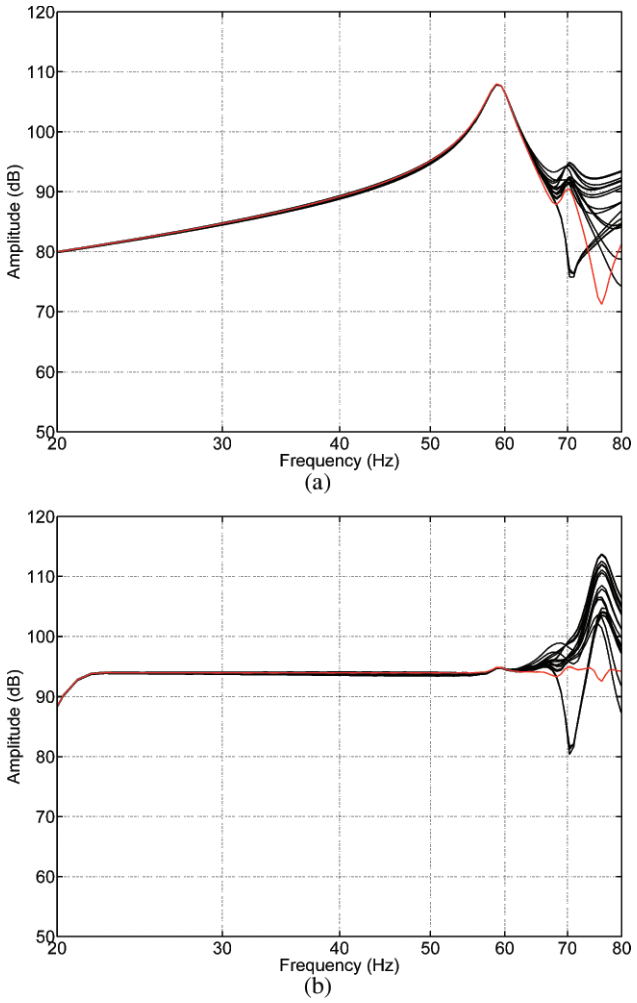

Fig. 19. Simulated frequency response over 25 listening points with four omnidirectional subwoofers at (0.4 m, 2.0 m, 0.4 m), (4.6 m, 2.0 m, 0.4 m), (2.5 m, 0.4 m, 0.4 m), and (2.5 m, 3.6 m, 0.4 m). (a) No equalization. (b) Single-point equalization at red line.

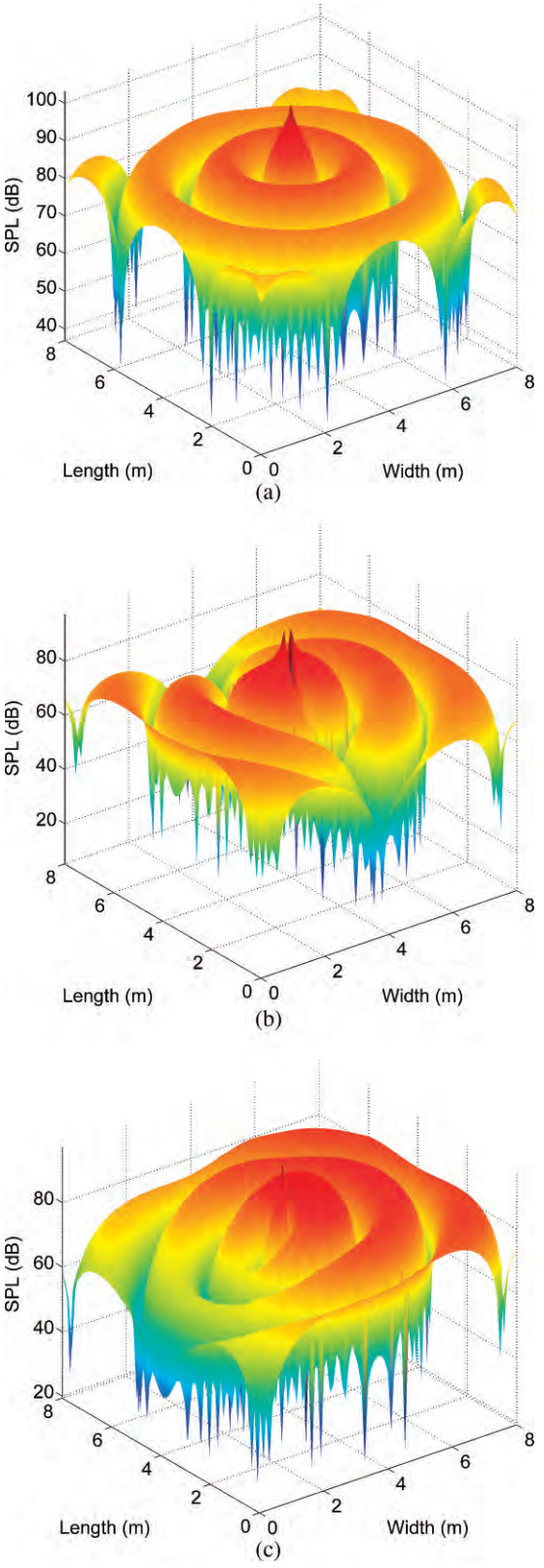

Fig. 20. Examples of polar pattern control. (a) Omnidirectional. (b) Dipole. (c) Cardioid.

simple example is given in Fig. 21 with an 0.8 m by 0.8 m sealed enclosure driven at 250 and 800 Hz.

It is possible to examine a nonrectangular enclosure configuration, such as an arbitrary elliptical design (Fig. 22). This can help examine whether a special enclosure design will reduce diffraction, giving a more even polar pattern. The example highlighted in Fig. 22 shows a decrease in diffraction at both 250 and 800 Hz due to the rounded shape of the enclosure, reducing the diffraction effects caused by sharp cabinet edges [17], [18].

The lower frequency range experiences a different effect from diffraction due to the longer wavelengths, resulting in closer similarity in phase of the diffracted field to the direct sound. In this frequency band diffraction will cause a shift in the acoustic center of the loudspeaker. This concept has been explored by Vanderkooy [19], [20], showing that below 200 Hz cabinet diffraction causes the acoustic center to be located a distance in front of the drive unit, relative to the front surface width and cabinet depth [20]. An example of this effect is given in Fig. 23, which shows a 0.5 by 0.5 m enclosure driven at 50 Hz.

4.5 Room Error-Correction Method Development

The toolbox can be used to model prototype signal-processing strategies to correct for response errors caused by room acoustics. A correction method contained within a standalone function can be implemented as a plug-in to the simulation, allowing the technique to be modified and fine-tuned within its own file without the need to modify the simulation code.

This capability was utilized by the authors to develop a novel room-correction concept utilizing adaptive networked subwoofer arrays that adjust themselves to their surroundings to give minimal spatial variance and maximum waveform integrity within a defined listening

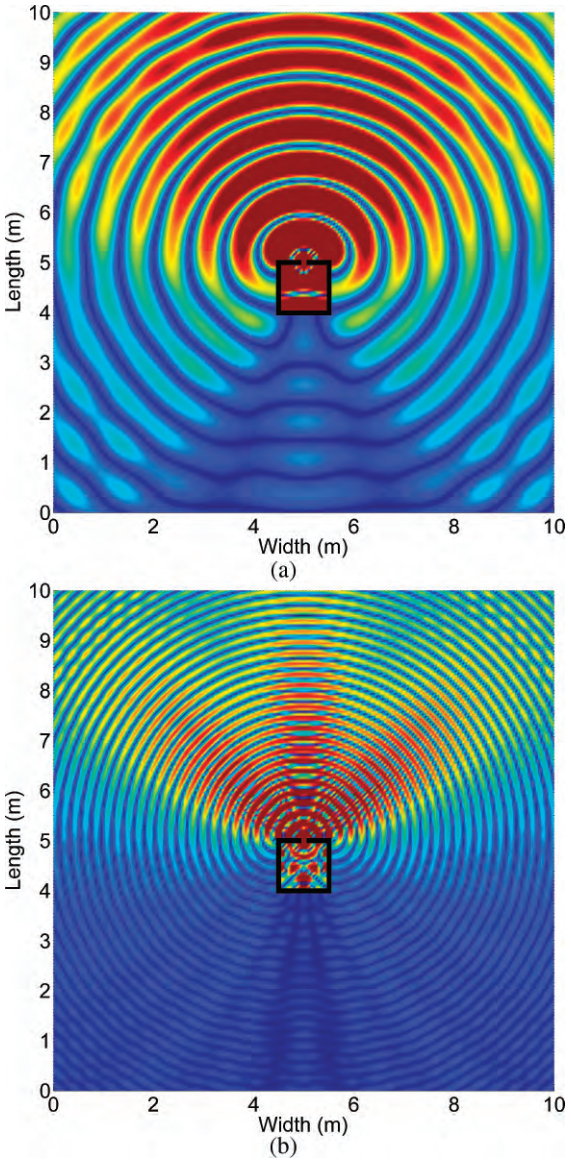

Fig. 21. Simulation of rectangular sealed enclosure. (a) At 250 Hz. (b) At 800 Hz.

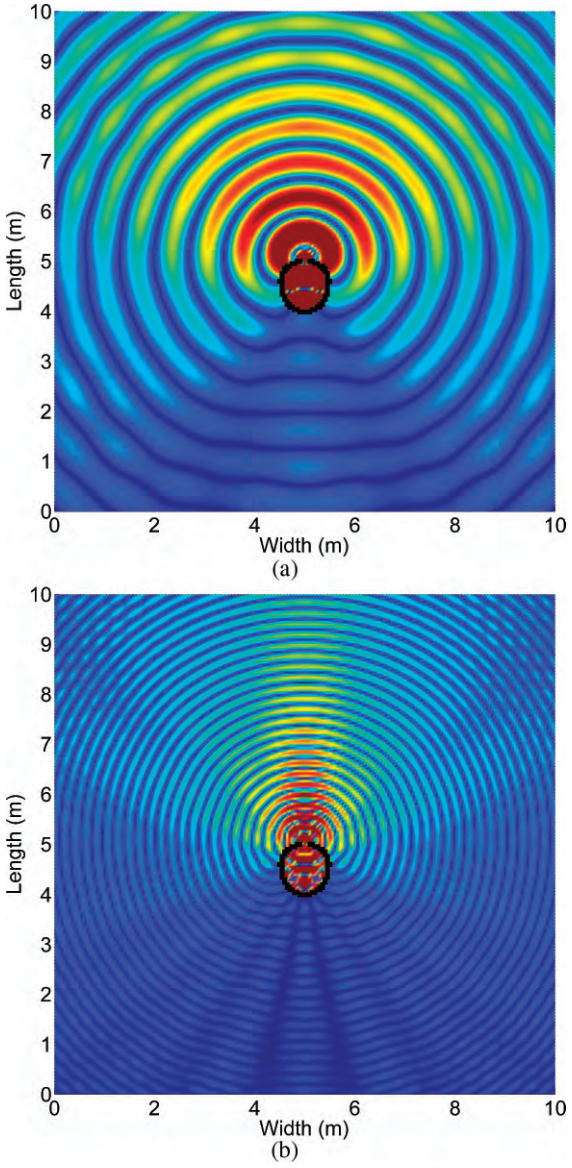

Fig. 22. Simulation of elliptical enclosure. (a) At 250 Hz. (b) At 800 Hz.

area. These arrays are referred to as chameleon subwoofer arrays [6]. The method can be evaluated within the toolbox in a number of ways. For example, a virtual walking path can be defined within the listening area, simulating an individual walking through the listening area, allowing users (listeners) to judge the level of variance within the listening space (Fig. 24).

In addition to the walking tests, the previously explored analysis options can be used to give further insight into the capabilities of the new concept. Impulse measurements can be used to determine magnitude deviation and spatial variance levels (Fig. 25) while a swept sinusoid signal can be utilized along with the spectrogram function to compare responses at listening locations. Upon achieving desirable results in the virtual environment, these conceptual correction methods can be transformed into the real world with a reasonable confidence level in terms of system performance.

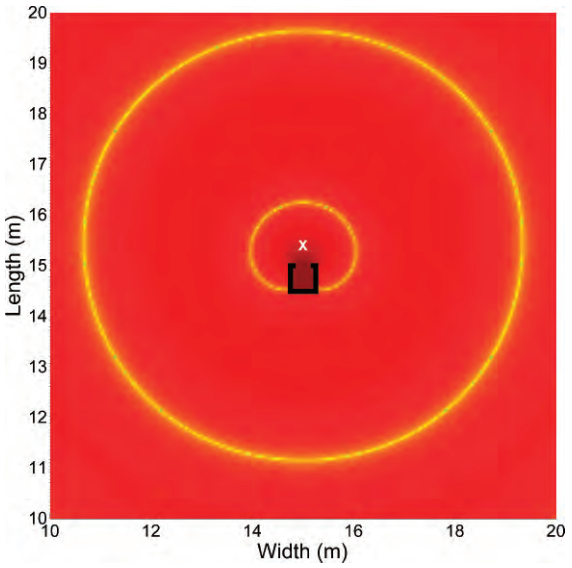

Fig. 23. Simulation of 0.5 by 0.5 m rectangular enclosure at 50 Hz showing a forward acoustical center shift, indicated by ×.

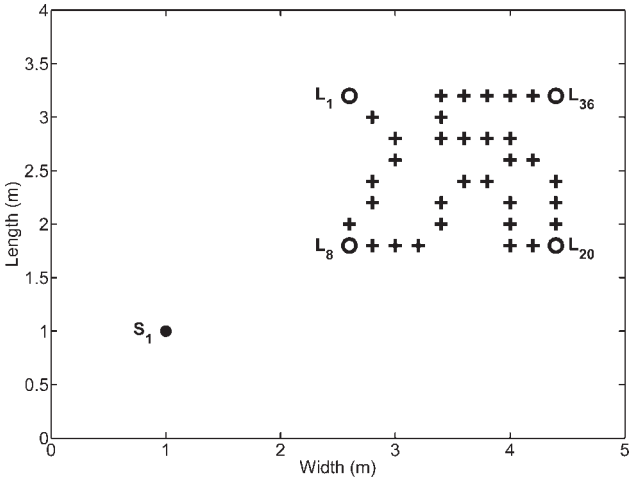

Fig. 24. Example of walking path test to judge performance of room correction method.

4.6 Large-Scale Sound Reinforcement Applications

Aside from small-room acoustics, large-scale sound reinforcement applications can be assessed within the toolbox. While large indoor and outdoor venues generally do not exhibit significant low-frequency variation across the audience due to room modes, deviations do exist due to large spacing of multiple subwoofer system components. This results in large nodal planes within the audience area, causing uneven low-frequency levels.

Another common requirement in these applications is to limit low-frequency energy on the stage to give musicians a reasonable and safe working environment. These two requirements cannot usually be met in precisely the same manner at each venue. Thus a toolbox

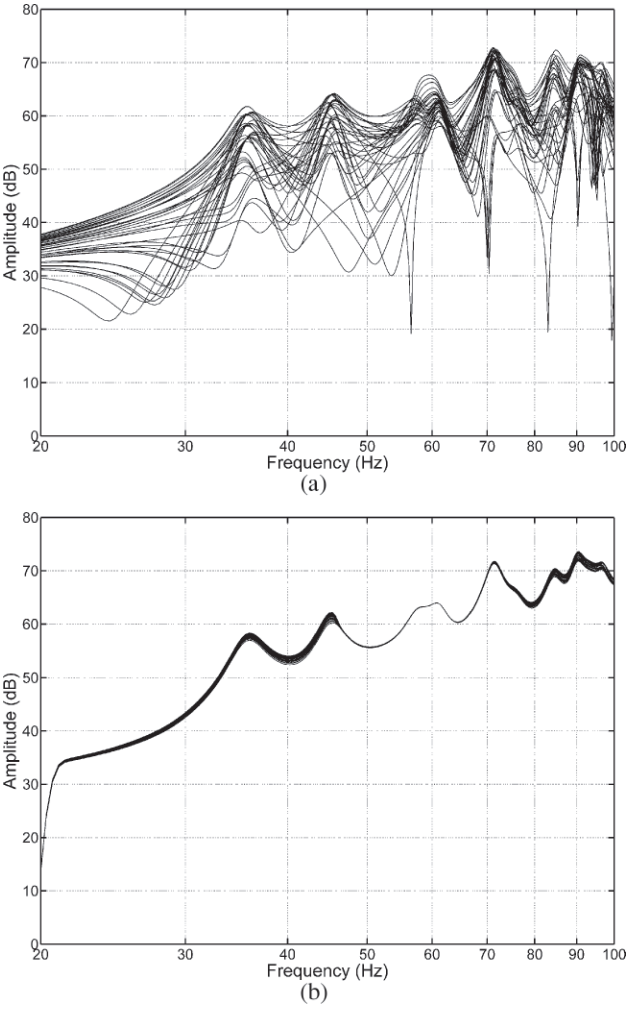

Fig. 25. Room responses, using a chameleon subwoofer array, over a 36-point listening grid. (a) Uncorrected. (b) Corrected.

with the ability to model each venue to allow for virtual fine-tuning of the subwoofer system can save time and money.

The toolbox embeds two routines to assist in this fine-tuning. First a cluster of four cardioid subwoofers [15] (Fig. 26) can be calibrated to give the appropriate audience coverage while minimizing stage levels [Fig. 27(a)]. Cardioid subwoofer clusters are used for this routine as they directly relate to what is used in practice [7]. Once the cluster configuration is set, the individual cluster components can be adjusted in the virtual environment to achieve the target audience coverage and stage rejection [Fig. 27(b)]. It has been suggested that well-planned subwoofer configurations can outperform systems consisting of a large number of arbitrarily placed subwoofers [7]. This saves truck space, fuel costs, setup time, and amplification/processing requirements while providing acceptable low-frequency behavior.

5 CONCLUSIONS

An acoustics simulation toolbox has been presented that utilizes the low-frequency accuracy of the FDTD method. The toolbox can handle the simulation of any two- or three-dimensional spatial configuration with very flexible parameters controlling the source(s), virtual measurements, and analysis options.

A key feature is the ability to visualize a sound wave propagating through a space over time where efficient computation enables fast animation of wave propagation. This allows for a close examination of room mode spatial distribution and interaction (if any) between the sound waves and any room obstacles. Used in conjunction with the various analysis options, the simulation toolbox allows for the proper design and configuration of a listening space, subwoofer system, and correction method with the ability to inspect the layout and response in a virtual environment before committing resources to build a physical system.

6 REFERENCES

[1] A. Taflove and S. C. Hagness, *Computational Electrodynamics: The Finite-Difference Time-Domain Method*, 3rd ed. (Artech House, Boston, MA, 2005).

[2] S. K. Olesen, "Low-Frequency Room Simulation Using Finite Difference Equations," presented at the 102nd Convention of the Audio Engineering Society, *J. Audio Eng. Soc*. (*Abstracts*), vol. 45, p. 405 (1997 May), preprint 4422.

[3] A. Celestinos and S. Birkedal Nielsen, "Multi-Source Low Frequency Room Simulation Using Finite Difference Time Domain Approximations," presented at the 117th Convention of the Audio Engineering Society, *J. Audio Eng. Soc*. (*Abstracts*), vol. 53, pp. 105, 106, (2005 Jan./Feb.), convention paper 6264.

[4] K. Kowalczyk and M. van Walstijn, "Modeling Frequency-Dependent Boundaries as Digital Impedance Filters in FDTD and K-DWM Room Acoustics Simulations," *J. Audio Eng. Soc*., vol. 56, pp. 569–582 (2008 July/Aug.).

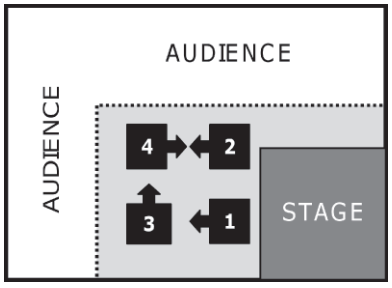

Fig. 26. Subwoofer cluster setup. Arrows indicate cardioid subwoofer orientation [7].

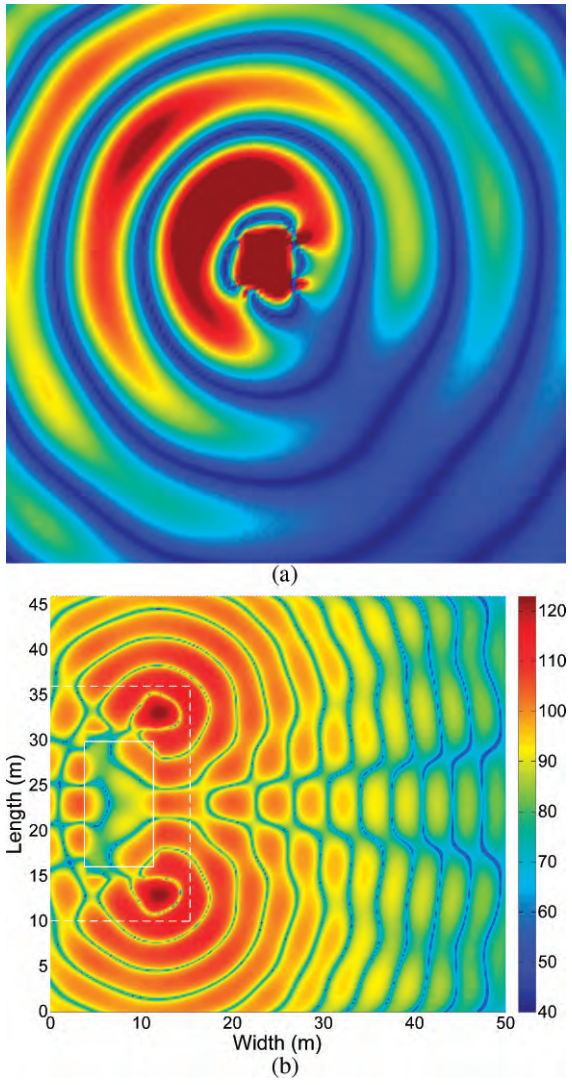

Fig. 27. (a) Simulation of single subwoofer cluster (linear pressure scale). (b) Resulting low-frequency coverage with two mirrored clusters on opposite corners of stage (logarithmic pressure scale) [7].

[5] J. G. Tolan and J. B. Schneider, "Locally Conformal Method for Acoustic Finite Difference Time-Domain Modeling of Rigid Surfaces," presented at the 140th Meeting of the Acoustical Society of America (2003 July 27).

[6] A. J. Hill and M. O. J. Hawksford, "Chameleon Subwoofer Arrays—Generalized Theory of Vectored Sources in a Closed Acoustic Space," presented at the 128th Convention of the Audio Engineering Society, (*Abstracts*) www.aes.org/events/128/128thWrapUp.pdf, (May 2010), convention paper 8074.

[7] A. J. Hill and M. O. J. Hawksford, "Subwoofer Positioning, Orientation and Calibration for Large-Scale Sound Reinforcement," presented at the 128th Convention of the Audio Engineering Society, (*Abstracts*) www.aes.org/events/128/128thWrapUp.pdf, (May 2010), convention paper 7971.

[8] FDTD Simulation Toolbox v8.0, www.adamjhill.com/fdtd.

[9] C. E. Shannon, "Communication in the Presence of Noise," *Proc. IRE*, vol. 37, pp. 10–21 (1949 Jan.).

[10] MATLAB version 7.6.0 (The MathWorks Inc., Natick, MA, 2008).

[11] A. Celestinos and S. Birkedal Nielson, "Optimizing Placement and Equalization of Multiple Low Frequency Loudspeakers in Rooms," presented at the 119th Convention of the Audio Engineering Society, *J. Audio Eng. Soc*. (*Abstracts*), vol. 53, p. 1206 (2005 Dec.), convention paper 6545.

[12] F. E. Toole, *Sound Reproduction: Loudspeakers and Rooms* (Focal Press, New York, 2008).

[13] T. Welti and A. Devantier, "Low-Frequency Optimization Using Multiple Subwoofers," *J. Audio Eng. Soc*., vol. 54, pp. 347–364 (2006 May).

[14] R. Walker, "Low-Frequency Room Responses: Part 2—Calculation Methods and Experimental Results," Rept. RD 1992/9, BBC Research Dept. (1992).

[15] H. F. Olson, "Gradient Loudspeakers," *J. Audio Eng. Soc*., vol. 21, pp. 86–93 (1973 Mar.).

[16] K. R. Holland, "A Simple Model of Cabinet Edge Diffraction," in *Reproduced Sound 2010*, vol. 32, pt. 5 (Proc. Institute of Acoustics, 2010 Nov.).

[17] R. M. Bews and M. O. J. Hawksford, "Application of the Geometric Theory of Diffraction (GTD) to Diffraction at the Edges of Loudspeaker Baffles," *J. Audio Eng. Soc*., vol. 34, pp. 771–779 (1986 Oct.).

[18] J. Eargle, *Loudspeaker Handbook*, 2nd ed. (Kluwer Academic, Boston, MA, 2003).

[19] J. Vanderkooy, "Applications of the Acoustic Centre," presented at the 122nd Convention of the Audio Engineering Society, (*Abstracts*) www.aes.org/events/122/122ndWrapUp.pdf, (2007 May), convention paper 7102.

[20] J. Vanderkooy, "The Low-Frequency Acoustic Centre: Measurement, Theory and Application," presented at the 128th Convention of the Audio Engineering Society, (*Abstracts*) www.aes.org/events/128/128thWrapUp.pdf, (May 2010), convention paper 7992.

THE AUTHORS

A. J. Hill

M. O. J. Hawksford

Adam J. Hill received a B.S. degree in electrical engineering from Miami University in 2007 and an M.Sc. degree with distinction in acoustics and music technology from the University of Edinburgh, Scotland, in 2008. He is currently pursuing a Ph.D. degree within the Audio Research Laboratory at the School of Computer Science and Electronic Engineering, University of Essex, Colchester, UK. His research focuses on the use of networked subwoofer arrays to control low-frequency room responses. Past research has included voice-coil temperature effects in loudspeakers and real-time equestrian horse tracking via GPS/IMU integration. Outside of school he works professionally as a live sound engineer for Gand Concert Sound.

Mr. Hill is a student member of the Audio Engineering Society, IEEE, IOA, and IET.

●

Malcolm O. J. Hawksford received a B.Sc. degree with first-class honors in 1968, a Ph.D. degree in 1972, and a D.Sc. degree in 2008, all from Aston University, Birmingham, UK.

He is currently a Professor within the School of Computer Science and Electronic Engineering at Essex University, Colchester, UK. Early research embraced delta and sigma–delta modulation (SDM) applied to color TV coding, which under the award of a BBC Research Scholarship led to a method of luminance and chrominance multiplexing exploiting digital time compression, a forerunner of MAC/DMAC. Current interests include audio engineering, electronic circuit design, and signal processing focused on loudspeakers, SDM, PWM linearization, spatial audio, and telepresence.

Dr. Hawksford is a recipient of the AES Publications Award for the best contribution by an author of any age to the *Journal*, volumes 45 and 46, and holds the AES Silver Medal for major contributions to engineering research in the advancement of audio reproduction. He is a chartered engineer and Fellow of the Audio Engineering Society, IET, and IOA. He has been chair of the AES Technical Committee on High-Resolution Audio and was a founding member of Acoustic Renaissance for Audio (ARA).